

## GAS-POWDER FLOW IN BLAST FURNACE WITH DIFFERENT SHAPES OF COHESIVE ZONE

X. F. DONG<sup>1</sup>, D. PINSON<sup>1</sup>, S. J. ZHANG<sup>1\*</sup>, A. B. YU<sup>1</sup>, P. ZULLI<sup>2</sup>

<sup>1</sup> School of Materials Science and Engineering, University of New South Wales, Sydney NSW 2052, Australia

<sup>2</sup> BHP Steel Research Laboratories, P.O. Box 202, Port Kembla, NSW 2505, Australia

### ABSTRACT

With high PCI rate operations, a large quantity of unburned coal/char fine will flow together with the gas into the furnace. Under some operating conditions, the hold-up of fines results in deterioration of furnace permeability and lower production efficiency. Therefore, it is important to understand the behaviour of powder (unburnt coal/char) inside the blast furnace when operating with different cohesive zone (CZ) shapes. This work is mainly concerned with the effect of cohesive zone shape on the powder flow and accumulation in a blast furnace. A model is presented which is capable of simulating a clear and stable accumulation region in the lower central region of furnace. The results indicate that powder is likely to accumulate at the lower part of W-shaped CZs and the upper part of V- and inverse V-shaped CZs. For the same CZ shape, a thick cohesive layer can result in a large pressure drop while the resistance of narrow cohesive layers to gas-powder flow is found to be relatively small. Implication of the findings to blast furnace operation is also discussed.

### NOMENCLATURE

- c compaction modulus (—)  
 C<sub>d</sub> drag coefficient (—)  
 d diameter, m  
 D\* hydrodynamic equivalent diameter,  
 $D^* = 2\phi_s d_s (1 - \varepsilon_s) / 3\varepsilon_s$ , m  
 F interaction force per unit volume, kg·m<sup>-2</sup>·s<sup>-2</sup>  
 F<sub>r</sub> Froude number,  $F_r = u_f / (D^* g)^{0.5}$   
 g gravitational acceleration, m·s<sup>-2</sup>  
 G mass flowrate, kg·m<sup>-2</sup>·s<sup>-1</sup>  
 G<sub>0</sub> normalizing unit factor, Pa  
 p pressure, Pa  
 Re<sub>r</sub> Reynolds number,  $Re_r = \phi_f d_f \rho_g \varepsilon_g |u_g - u_f| / \mu_g$   
 t time, s  
 u interstitial velocity, m·s<sup>-1</sup>  
 U superficial velocity, m·s<sup>-1</sup>

### Greek

- ε volume fraction (—)  
 ε\* Compaction volume fraction (—)  
 I identity tensor (—)  
 μ viscosity, kg·m<sup>-1</sup>·s<sup>-1</sup>  
 ρ density, kg·m<sup>-3</sup>  
 τ stress tensor, Pa  
 φ shape factor (—)

### Subscripts

- g gas

- f powder  
 fd dynamic powder  
 fs static powder  
 s solid

### Superscripts

- max maximum

### INTRODUCTION

An ironmaking blast furnace is a complex reaction vessel involving counter-, co- and/or cross-current flows of gas, powder, liquid, and solids. It is important to understand the multiphase flow to develop effective methods for process control. The particular interest here is the transport phenomena of powder in the blast furnace. The development of Pulverised Coal Injection (PCI) has led to a reduction in coke consumption and hence production cost. While this technology has been widely applied to blast furnace operations, it causes a number of changes to the furnace behaviour, some of which can be detrimental. For example, high PCI rates can result in powder, i.e. ash and partially burnt coal char, entering the furnace together with the gas flow. Under some conditions, powder can accumulate in the shaft and lower zones reducing the permeability and resulting in problems in gas flow and liquid drainage. Such accumulation has been reported as a limiting factor for increasing PCI rate (Yamaguchi et al., 1992).

Due to the difficulty of online sampling in an operating blast furnace, numerical simulation of gas-powder flow processes provides a basic tool for design and optimization. In the past, various models have been proposed (Fan et al., 1983; Yamaoka, 1986; Shibata et al., 1991; Van der Ham et al., 1993; Yagi, 1993; Chen et al., 1994; Sugiyama, 1996) to describe the gas and powder flow, where the powder phase is treated as a continuous medium with properties analogous to those of a fluid. However, there is still poor agreement among these published studies of powder hold-up distribution. Our recent study indicates that a fully filled powder accumulation region can be formed in laboratorial scale 2D packed bed (Dong, Pinson et al., 2003), which has not been considered in the previous work. A two fluid model has been proposed to numerically describe the phenomena of powder accumulation (Dong, Zhang et al., 2003).

In this work, that model is applied to investigate the flow behaviour and accumulation characteristics of powder within a BF. The model used permits the insertion of dummy cells to represent typical cohesive zones and determines the localized flow and accumulation of powder, providing a convenient way to predict the powder holdup distribution and hence the performance of BF.

\* Present addresses of: CFD Research Corporation, 215 Wynn Dr., Huntsville, AL 35805, USA

## MATHEMATICAL MODELLING

### Governing equations

A model for gas–powder two-phase incompressible flow in a packed bed can be formulated based on the space-averaged theorem (Soo, 1967; Ishii, 1975). The phases are described in terms of separate conservation equations with a shared pressure and appropriate interaction terms representing the coupling between the phases. Meanwhile, the irregular geometry of a packed bed is treated as an isotropic porous media. The influence of packed particles is taken into account in the model through the bed voidage and its interactions with gas and powder phases. Thus, we have following governing equations:

Gas phase:

$$\frac{\partial \varepsilon_g}{\partial t} + \nabla \cdot (\varepsilon_g \mathbf{u}_g) = 0 \quad (1)$$

$$\frac{\partial (\rho_g \varepsilon_g \mathbf{u}_g)}{\partial t} + \nabla \cdot (\rho_g \varepsilon_g \mathbf{u}_g \mathbf{u}_g) = -\varepsilon_g \nabla p + \nabla \cdot \boldsymbol{\tau}_g + \rho_g \varepsilon_g \mathbf{g} + \mathbf{F}_g^s + \mathbf{F}_g^f \quad (2)$$

Powder phase:

$$\frac{\partial \varepsilon_{fd}}{\partial t} + \nabla \cdot (\varepsilon_{fd} \mathbf{u}_f) = 0 \quad (3)$$

$$\frac{\partial (\rho_f \varepsilon_{fd} \mathbf{u}_f)}{\partial t} + \nabla \cdot (\rho_f \varepsilon_{fd} \mathbf{u}_f \mathbf{u}_f) = -\varepsilon_{fd} \nabla p + \nabla \cdot \boldsymbol{\tau}_f + \rho_f \varepsilon_{fd} \mathbf{g} + \mathbf{F}_f^s + \mathbf{F}_f^g \quad (4)$$

where

$$\varepsilon_s + \varepsilon_g + \varepsilon_{fd} + \varepsilon_{fs} = 1$$

The constitutive equations necessary for closure of the above equations are listed in Table 1.

**Table 1:** Constitutive equations

$$\begin{aligned} \boldsymbol{\tau}_g &= -\frac{2}{3} \varepsilon_g \mu_g (\nabla \cdot \mathbf{u}_g) \mathbf{I} + \varepsilon_g \mu_g [(\nabla \mathbf{u}_g) + (\nabla \mathbf{u}_g)^T] \\ \boldsymbol{\tau}_f &= -\left[ p_f + \frac{2}{3} \varepsilon_{fd} \mu_f (\nabla \cdot \mathbf{u}_f) \right] \mathbf{I} + \varepsilon_{fd} \mu_f [(\nabla \mathbf{u}_f) + (\nabla \mathbf{u}_f)^T] \\ \mathbf{F}_g^s &= -\mathbf{F}_s^g = -\left[ 150 \frac{(\varepsilon_s + \varepsilon_{fs})^2}{\varepsilon_s + \varepsilon_{fd}} \frac{\mu_g}{(\phi_s d_s)^2} + 1.75 (\varepsilon_s + \varepsilon_{fs}) \frac{\rho_g}{\phi_s d_s} \right] |\mathbf{u}_s - \mathbf{u}_f| (\mathbf{u}_s - \mathbf{u}_f) \\ \mathbf{F}_f^g &= -\mathbf{F}_f^s = -\frac{3}{4} C_d \frac{\varepsilon_g \rho_g \varepsilon_{fd}}{\phi_f d_f} |\mathbf{u}_g - \mathbf{u}_f| \varepsilon_g^{-2.65} (\mathbf{u}_g - \mathbf{u}_f) \\ \text{where } C_d &= \begin{cases} \frac{24}{\text{Re}_f} \dots \dots \dots \text{Re}_f \leq 1 \\ \frac{24}{\text{Re}_f} [1 + 0.15 \text{Re}_f^{0.687}] \dots \dots 1 < \text{Re}_f \leq 1000 \\ 0.44 \dots \dots \dots 1000 < \text{Re}_f \end{cases} \\ \mathbf{F}_f^s &= -\frac{7.49}{D} \frac{\rho_f \varepsilon_{fd}}{\text{Fr}_f^{1.33}} |\mathbf{u}_f - \mathbf{u}_s| (\mathbf{u}_f - \mathbf{u}_s) \\ p_f &= \frac{G_0}{c} \exp[c(\varepsilon_{fd} - \varepsilon_f^*)] \end{aligned}$$

### Numerical solution

The two sets of conservation equations, closed by the constitutive equations and supplemented with the initial and boundary conditions, can only be solved numerically. To date, two common algorithms for sequential iterative multi-phase control volume solvers are the InterPhase Slip Algorithm (Spalding, 1983) and the Implicit MultiField (IMF) method (Harlow, 1975), of which the treatment here is based on the more implicit IPSA algorithm enhanced with Partial Elimination Algorithm (PEA) which was

implemented to de-couple the drag and accelerate convergence. The calculation domain is represented by a number of fixed Eulerian cells through which the gas-powder dispersion moves. A non-staggered grid was utilized, complimented with the Rhie-Chow scheme (Rhie and Chow, 1983) to eliminate non-physical oscillations of pressure field. For the discretization of the convective terms in the conservation equations, the deferred correction technique (Khosla and Rubin, 1974) has been used, which is a lower-order approximation plus difference between explicit higher order and explicit lower order approximations.

It has been realized that when powder is injected into a packed bed, some is entrained by the gas and some is entrapped by the particles packed. The volume fraction of the entrained powder is referred to as the dynamic holdup, and the entrapped powder as the static holdup. In this work, it is assumed that the static powder is quantified by the following equation, modified from that of Hidaka et al. (1998):

$$\varepsilon_{fs} = \text{Min} \left\{ 1.6 \times 10^{-4} \left[ 1 + 0.006 (\text{U}_g / d_s)^{0.4} \right]^{2.5} G_g^{-3.0}, \varepsilon_f^{\text{max}} \right\} \quad (5)$$

This equation implies that there is a maximum powder holdup  $\varepsilon_f^{\text{max}}$  that corresponds to the situation when the voids among packed particles are fully occupied by powder particles. A region with maximum holdup, i.e. the powder accumulation region, will not allow any powder to penetrate, thus providing a boundary to the powder phase, although gas can still flow through it. This region may form gradually until a steady flow for both gas and powder phases is reached. Therefore, to determine this accumulation region and gas-powder flow simultaneously, the following solution technique has been used in this work which is mainly concerned with the final, steady state flow for given flow conditions:

1. Determine the (initial) gas and powder flow fields under the boundary conditions at the inlet, outlet and walls;
2. Determine powder accumulation regions based on powder volume fraction;
3. Calculate the gas and powder flow fields, with the profile of accumulation region as part of the boundaries for powder phase;
4. Step 3 is continued until steady-state flow is reached;
5. Repeat Steps 2-4 to achieve a converged accumulation region.

## RESULT AND DISCUSSION

### Validation of the present model

Experiments have been carried out under the conditions listed in Table 2. The 2D packed bed used is rectangular with the dimensions of 100 mm in width, 300 mm in height and 10 mm in thickness, respectively. The air and powder are injected through a lateral inlet (25 mm in height, 10 mm full bed thickness). The front side of the bed is made of clear acrylic sheet so that a digital video camera can be used to record the events. Fig. 1(a) illustrates a typical steady experimental result. An accumulation region (white part) can be observed in the corner opposite to the inlet. The calculated total hold-ups

in terms of powder volume fraction contours are shown in Fig. 1(b).

**Table 2:** Conditions for the validation experiment

Variables	Present Study
Particle diameter $d_s$ (mm)	3 (GB)
Mean powder diameter $d_f$ (mm)	0.075 (GP)
Bed voidage	0.40
Gas density $\rho$ ( $\text{kg}\cdot\text{m}^{-3}$ )	1.177
Gas viscosity $\mu$ ( $\text{kg}\cdot\text{m}^{-1}\cdot\text{s}^{-1}$ )	$1.86\times 10^{-5}$
Powder density ( $\text{kg}\cdot\text{m}^{-3}$ )	2500
Superficial gas velocity $U_g$ ( $\text{m}\cdot\text{s}^{-1}$ )	0.417 (no block), 0.5 (inverse V CZ)
Powder mass flux $G_f$ ( $\text{kg}\cdot\text{m}^{-2}\cdot\text{s}^{-1}$ )	0.51
Gas Reynolds number ( $Re_g=\rho u_g d_s/\mu$ )	79, 95

GB: Glass Beads; GP: Glass Powder

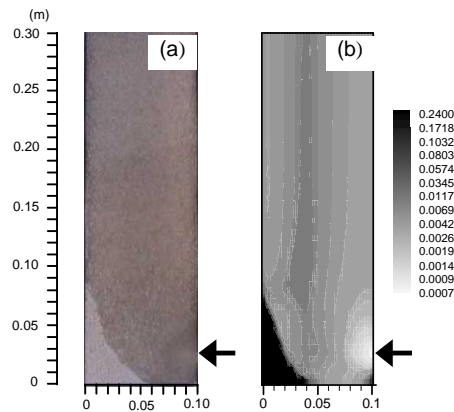


**Figure 1:** Comparison between experimental and calculated powder accumulation region when  $U_g = 0.417 \text{ m}\cdot\text{s}^{-1}$ ,  $G_f=0.51 \text{ kg}\cdot\text{m}^{-2}\cdot\text{s}^{-1}$ : (a), experimental; (b), calculated.

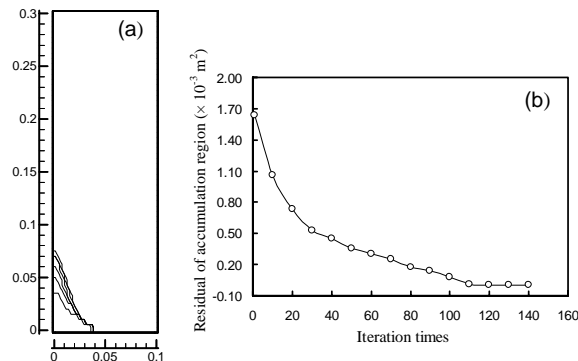


**Figure 2:** Convergence of the accumulation region profile under conditions same as those in Fig. 1 (b).

For the conditions of Fig. 1, Fig. 2(a) shows calculated accumulation region profiles at twenty iteration intervals. The residuals for the accumulation region are shown in Fig. 2(b) indicating that a converged accumulation region profile can be achieved after a small number of iterations. In the computation, the limiting volume fraction of 0.24 in the accumulation region is obtained by assuming that the voidage of the packing is initially 0.4 and the maximum powder volume fraction in the void is 0.6 (Therefore the criterion for powder accumulation is  $0.4\times 0.6=0.24$ ). It can be observed from comparison of Figs. 1 and 2, that there is reasonable agreement between the calculated and measured powder accumulation regions in size and shape. A sharp gradient interface exists between the calculated

powder accumulation region and the bed. This compares well to the experimental results. Good agreement can also be found for a bed with inserted blocks simulating fused layers in a CZ as shown in Fig. 3.

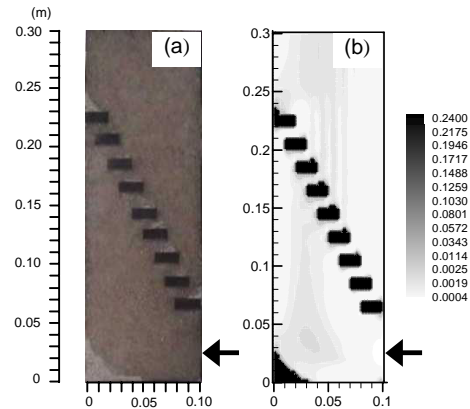


**Figure 3:** Comparison between experimental and calculated powder accumulation regions in inverse V-shaped CZ when  $U_g = 0.5 \text{ m}\cdot\text{s}^{-1}$ ,  $G_f = 0.51 \text{ kg}\cdot\text{m}^{-2}\cdot\text{s}^{-1}$ : (a), experimental; (b), calculated.

### Simulations with different CZ structures

#### (1) Simulation conditions

As shown in Table 3, numerical simulations have been performed under conditions similar to a BF with approximately  $1000 \text{ m}^3$  inner volume (hearth diameter: 7.2 m, height: 25 m). Different CZ shapes (inverse V, W and V) are employed in this study to investigate the effect of CZ structure on gas and powder flow. In practice, the CZ layers are impermeable to gas flow (Omori, 1987) and are modelled by a series of dummy cells in the simulation.

**Table 3:** Simulation conditions

Variables	Blast furnace
Particle diameter $d_s$ (mm)	25
Powder diameter $d_f$ (mm)	0.075
Bed voidage	0.4
Gas density $\rho$ ( $\text{kg}\cdot\text{m}^{-3}$ )	1.25
Gas viscosity $\mu$ ( $\text{kg}\cdot\text{m}^{-1}\cdot\text{s}^{-1}$ )	$1.8\times 10^{-5}$
Powder density ( $\text{kg}\cdot\text{m}^{-3}$ )	1400
Superficial gas velocity $U_g$ ( $\text{m}\cdot\text{s}^{-1}$ )	0.976
Powder mass flux $G_f$ ( $\text{kg}\cdot\text{m}^{-2}\cdot\text{s}^{-1}$ )	0.154
Cohesive zone shapes	W, V, Inverse V

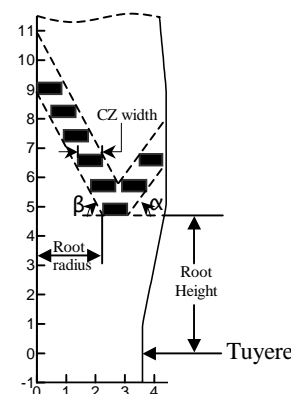


**Figure 4:** Definition of CZ parameters.

In this study, packing materials in the furnace are assumed to be composed of uniform ore and coke particles where spherical factor is 0.9. The effect of the particle diameter and geometry on the gas-powder flow has been considered in the interaction force between powder and particle. CZ is characterised by several parameters as shown Fig. 4. The root radius and height, CZ width, and the incline angles,  $\alpha$  and  $\beta$ . The ranges studied are detailed in Table 4.

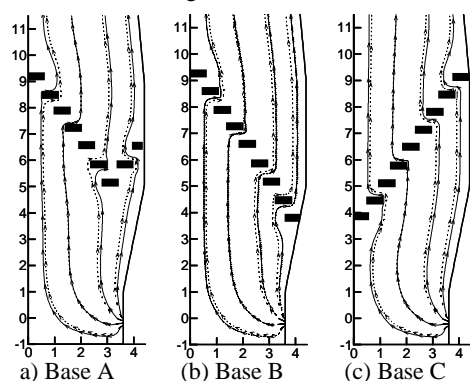
**Table 4:** Cases for simulation of powder flow in a BF

CZ	RH (m)	RR (m)	$\alpha$	$\beta$	Width (m)	Ratio
W-shaped						
Base A	5.1	2.75	55	55	0.6	1.0
Case 1	2.75	2.75	55	55	0.6	1.0
Case 2	5.1	2.8	55	55	0.36	1.0
Case 3	5.1	2.9	55	55	0.6	2.0
Inverse V-shaped						
Base B	3.75	3.50		55	0.6	1.0
V-shaped						
Base C	3.75	0	55		0.6	1.0

CZ: cohesive zone; RH: root height; RR: root radius;  $\alpha, \beta$ : inclined angle (degree); Width: width of single layer; Ratio: ratio of impermeable/permeable layer

## (2) Typical results under base conditions

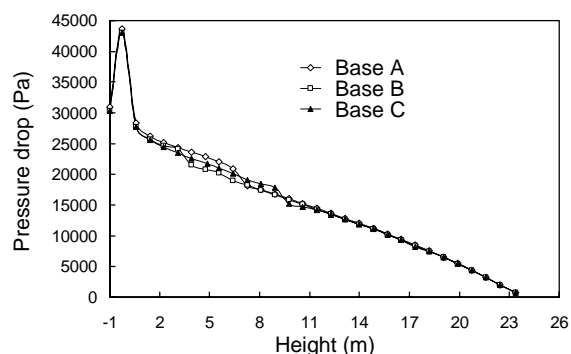
Simulations in this study demonstrate that the cohesive layers act as gas and powder distributor so that there are different flow trends below and above the CZs. For example, as shown in Fig. 5(b), above the inverse V-shaped cohesive layers, the streamlines turn toward the furnace wall away from the center of the furnace. However, below the cohesive layers, the flow is towards to the center of the furnace. The comparison for streamlines of the gas and powder phases shows that powder does not follow the gas flow exactly. Near the wall, the powder streamline is on the left of gas streamline due to the high powder flow inertia. Close to the center of furnace, powder flow lags behind gas flow so that powder streamline is inside the gas streamline.



**Figure 5:** Streamlines for different CZ shapes: — gas streamline; ..... powder streamline.

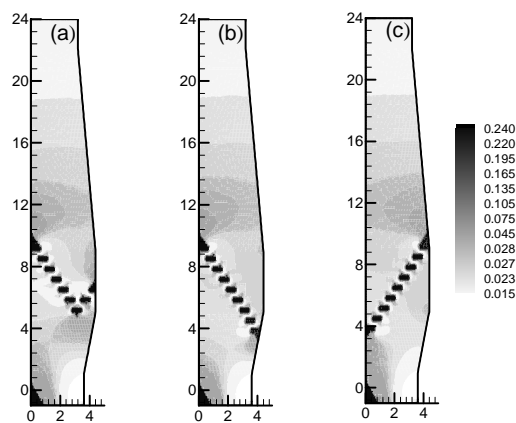
The effect of CZ shapes on pressure drop is shown in Fig. 6. The calculated pressure drop is relative to the outlet. The pressure profiles show little difference between the cases except in the region of the CZ. The phenomena also can be found in the central part of furnace. The comparison shows that the pressure drop for Inverse V-shaped CZ is the least. That is to say, the resistance of

inverse V-shaped CZ to gas-powder flow near the wall is relatively weak.



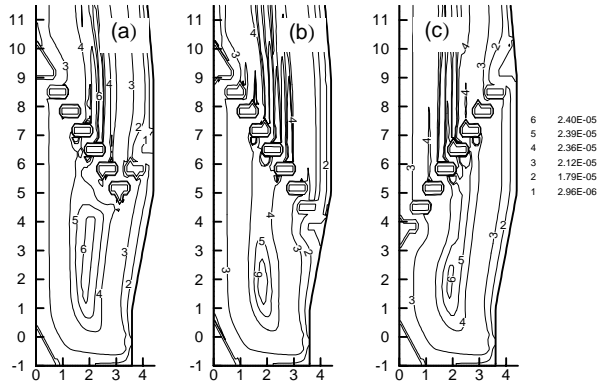
**Figure 6:** Pressure distribution along the wall.

The calculated total powder holdup distribution is shown in Fig. 7. A powder accumulation region can be identified in the lower part of the BF. For different CZ shapes, the powder distribution shows significant differences. For the W-shaped CZ, a relatively dense powder distribution occurs at the lowest part of the CZ. For the inverse-V shaped CZ, there is a denser powder distribution near the wall. Due to the characteristics of the V-shaped CZ, low gas velocity in the furnace center causes denser powder holdup in comparison to the other two shapes. Generally, powder is likely to accumulate in the low gas flow region as previously described [Sugiyama, 1996]. From the inlet to accumulation region, total powder holdup gradually becomes higher. In the CZ, the increased gas velocity induces low powder holdup in the coke slits between the impermeable fused ore layers. However, at the corner of some layers, powder can still accumulate due to the convergence of gas streamlines, such as the upper part of V- and inverse V-shaped CZs.



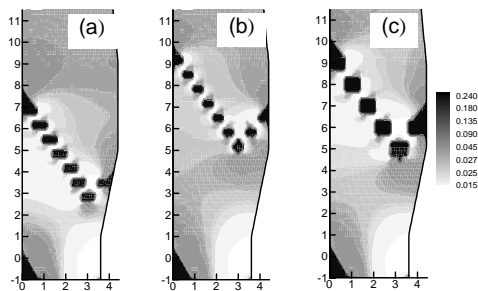
**Figure 7:** Computed powder total holdup for different CZ shapes: (a), Base A; (b), Base B; (c), Base C.

Fig. 8 shows the distribution of dynamic holdup. Below the CZs, the maximum dynamic holdup can be observed in the mid-radius region. The results show that the W CZ shape has a more uniform powder flow compared to other cases. Above the CZs, the contours of dynamic holdup appear to extend from the cohesive layers. This flow pattern looks like 'smoke bands'. These 'smoke bands' are located at the convergence of the streamlines of the powder flow and their appearances change with the CZ shape. Inverse V-shaped CZ 'smoke bands' deviate towards the wall. V-shaped CZ 'smoke bands' move to the center as the dynamic holdup is driven by the gas flow.



**Figure 8:** Computed dynamic holdup for the base conditions: (a), Base A; (b), Base B; (c), Base C.

**(3) Effect of CZ structure**

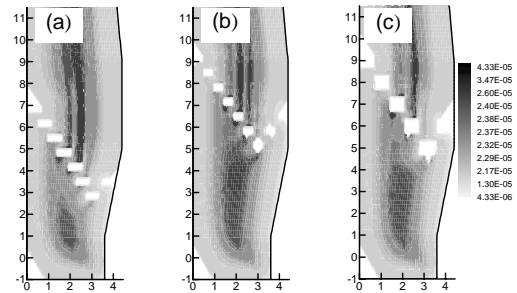


**Figure 9:** Total holdup distribution under various W-shaped CZs: (a), Case 1; (b), Case 2; (c), Case 3.

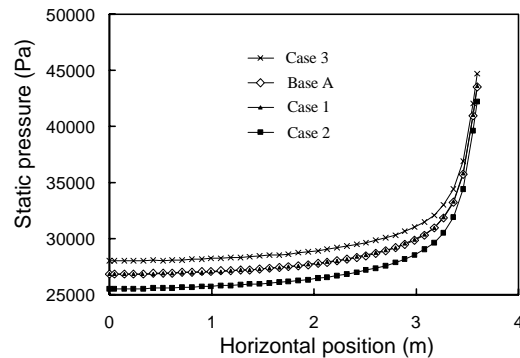
The structure of a CZ is controlled by the furnace productivity and charging patterns, etc. In this study, three cases with different incline angle, CZ height and width are considered to investigate the influence of W-shaped CZ structures on gas-powder flow. Fig. 9 shows how the total powder holdup distribution changes with the CZ structural parameters. Compared with the base case shown in Fig. 7(a), it can be seen that the distribution of powder holdup is significantly affected by the CZ structure. When the cohesive layers are lowered in the furnace, gas flow through the modeled ‘coke slits’ is quite strong and the cross flow of gas and powder becomes evident in the bosh so that relatively low powder accumulation can be observed in and around the cohesive layers compared to other cases. Fig. 9(c) shows the distribution of total holdup for thick cohesive layers. It appears that increased thickness of an impermeable layer does not seem to change the accumulation much. Compared to the base case, narrow cohesive layers will result in high powder holdup on the layers shown in Fig. 9(b) because the cross gas flow becomes weak due to the decreased width of cohesive layer.

Fig. 10 shows the dynamic holdup distribution of powder under conditions corresponding to Fig. 9. Different CZs split the powder holdup into the different kinds of bands so as to induce the re-distribution of ‘smoke bands’. Compared to the base condition (Fig. 8(a)), Fig. 10(a) shows that the spot for maximum dynamic holdup moves downward with the lower root of the CZ. However, there is nearly no change for the distribution of pressure loss between case 1 and the base case, which is shown in Fig. 11. This implies that a low CZ possibly does not

deteriorate the operational conditions in practice, at least for pressure loss. Similarly, in the simulation of single phase flow in blast furnace geometry with CZs, it has been reported that the effect of CZ height on pressure drop is insignificant (Omori, 1987). Fig. 10(b) shows that narrow cohesive layers result in straight ‘smoke bands’ above the layers and the spot for maximum dynamic holdup moves up compared to the base case. This indicates that the narrow layers make gas-powder flow through the slits easier. The resistance to flow becomes less so that the pressure loss is minimized among the calculated cases. Compared to the previous cases, increasing the thickness of impermeable layers (Fig. 10(c)) makes most of ‘smoke bands’ above the CZ blow off. Meanwhile, pressure drop becomes larger than the base case due to the decrease in total coke slit area.



**Figure 10:** Dynamic holdup distribution in blast furnace under various W-shaped CZs: (a), Case 1; (b), Case 2; (c), Case 3.



**Figure 11:** Comparison of horizontal distribution of pressure at the inlet level

The overall performance of the furnace is affected markedly by the location and magnitude of the resistances associated with the cohesive zones. Lowering of the cohesive zone, with a corresponding increase in the volume of the lumpy zone, has been found to be correlated with a decrease in wall temperature and a low silicon hot metal (Nikitin, 1992). A narrow cohesive zone maximizes permeability and thereby also productivity. An increase in blast volume raises the yield of gases in the lower part of the furnace, consequently raises the level of the cohesive zone. So, in the present work, the cases shown in Table 4 are closely related to furnace operation with complex CZ structures. Predicted powder accumulation region and powder holdup distribution results indicate that it is possible to link the current model with the operating conditions of the blast furnace, providing a convenient way to monitor changes of burden permeability in a blast

furnace. However, it should be pointed out that the present work focused on the effect of CZ characteristics ignoring the influence of liquid metal and slag flow and burden movement on powder distribution. There is still relatively limited understanding for the powder distribution in an actual blast furnace. The influence of the above factors will be studied more closely in subsequent work.

## CONCLUSION

A two-fluid flow model has been extended to simulate powder flow and distribution in the blast furnace. Its validity has been verified from the good agreement between measured and calculated results for different flow conditions. When applied to BF geometry, a relatively large total powder holdup can be numerically identified in the central region and lower part of the cohesive zone. The pattern of dynamic holdup varies with CZ shape. For a given CZ shape, thick impermeable layers can result in a large pressure drop and the resistance of CZs with narrow layers to gas and powder flow is relatively small.

## ACKNOWLEDGEMENTS

The authors are grateful to Australian Research Council and BHP Steel for the financial support of this work.

## REFERENCES

- CHEN, J., AKIYAMA, T., NOGAMI, H. AND YAGI, J. (1994), "Behavior of powders in a packed bed with lateral inlets", *ISIJ Int.*, **34**, 133-139.
- DONG, X.F., PINSON, D., ZHANG, S.J., YU, A.B. AND ZULLI, P. (2003), "Gas-powder flow and powder accumulation in a packed bed (part I): experimental study", UNSW internal report.
- DONG, X.F., ZHANG, S.J., PINSON, D., YU, A.B. AND ZULLI, P. (2003), "Gas-powder flow and powder accumulation in a packed bed (part II): numerical simulation", UNSW internal report.
- FAN, L-S., TODA, M. AND SATIJA, S. (1983), "Hold-up of fine particles in the packed dense bed of the multisolid pneumatic transport bed", *Powder Technology*, **36**, 107-114.
- HARLOW, F.H. AND AMSDEN, A.A., (1975), "Numerical calculation of multiphase fluid flow", *Journal of Computational Physics*, **17**, 19-52.
- ISHII, M., *Thermo Fluid Dynamic Theory of Two Phase Flow*, Eyrolles, 1975.
- NIKITIN, G.M., BELYAKOV, V.N. AND DANAIEV, N.T. (1992), 'Determination of blast furnace cohesive zone parameters', *Steel in Translation*, **22**, 159-162.
- OMORI, Y. (Editor), *Blast furnace phenomena and modelling*, Elsevier Applied Science, 1987.
- SHIBATA, K., SHIMIZU, M., INABA, S., TAKAHASHI, R. AND YAGI, J. (1991), "Pressure loss and hold up powders for gas-powder two phase flow in packed beds", *ISIJ Int.*, **31**, 434-439.
- SOO, S.L., *Fluid Dynamics of Multiphase System*, Blaisdell, Waltham, MA, 1967.
- SPALDING, D.B. (1980), "Numerical computation of multi-phase fluid flow and heat transfer", *Recent Advances in Numerical Methods in Fluids*, Taylor, C., Morgan, K. (editors), Swansea: Pineridge Press, 139-167.
- SUGIYAMA, T. (1996), "Experimental and numerical analysis on the movement and the accumulation of powder in the deadman and the dripping zone of blast furnace", *Tetsu-to-Hagané*, **82**, 29-34.
- VAN DER HAM, A. G. J. AND PRINS, W. AND VAN SWAAIJ, W. P. M. (1993), "Hydrodynamics of a pilot-plant scale regularly packed circulating fluidized bed", *AIChE Symposium Series*, **89**, 53-72.
- YAGI, J. (1993), "Mathematical modeling of the flow of four fluids in a packed bed", *ISIJ Int.*, **33**, 619-639.
- YAMAGUCHI, K., UENO, H. AND TAMURA, K. (1992), "Maximum injection rate of pulverized coal into blast furnace through tuyeres with consideration of unburnt char", *ISIJ Int.*, **32**, 716-724.
- YAMAOKA, H. (1986), "Flow characteristics of gas and fine particles in a two-dimensional space of packed bed", *Tetsu-to-Hagané*, **72**, 2194-2201.
- RHIE, C.M. AND CHOW, W.L. (1983), "A numerical study of the turbulent flow past an isolated airfoil with trailing edge separation", *AIAA Journal*, **21**, 1525-1532.
- KHOSLA, P.K., RUBIN, S.G. (1974), "A diagonally dominant second-order accurate implicit scheme", *Computers & Fluids*, **2**, 207-209.
- HIDAKA, N., IYAMA, J., MATSUMOTO, T., KUSAKABE, K. AND MOROOKA, S. (1998), "Entrainment of fine particles with upward gas flow in a packed bed of coarse particles", *Powder Technology*, **95**, 265-271.